



LIQUEFACTION- INDUCED LATERAL SPREADING FOR LARGE- MAGNITUDE SUBDUCTION EARTHQUAKES

W. Araujo ⁽¹⁾, C. Ledezma ⁽²⁾

⁽¹⁾ Ph.D. Student, Dept. of Structural and Geotechnical Engineering at Pontifical Catholic University of Chile, wsaraujo@uc.cl

⁽²⁾ Associate Professor, Dept. of Structural and Geotechnical Engineering at Pontifical Catholic University of Chile, ledezma@ing.puc.cl

Abstract

Recent earthquakes have reminded us that liquefaction-induced lateral spreading can generate significant deformations and damage in existing structures such as buildings, ports, and bridges. In the case of large-magnitude subduction earthquakes, such as those experienced in Chile, current empirical models tend to underestimate or overestimate (by a factor of two or more) actual field measurements. One of the reasons why this discrepancy takes place is because those models are derived from a database with different sources, fault types, and earthquakes magnitudes (typically below Mw 7.5). The purpose of this study is to identify ground motion intensity parameters that better predict liquefaction-induced lateral spreading, based on statistical trends derived from a parametric numerical modeling with a database of large magnitude ($M_w \geq 7.5$) subduction earthquakes occurred in Chile. In this study, a fully coupled finite-element model using a multi-yield surface plasticity constitutive model has been applied to numerically investigate the effects of different parameters not used in current models to predict lateral spread in subduction earthquakes. The numerical model was validated against centrifuge tests from literature and historical cases. The results revealed that Cumulative Absolute Velocity, Peak Ground Velocity and Arias Intensity have the strongest correlation with lateral spreading in large magnitude subduction earthquakes.

Keywords: Liquefaction, lateral spreading, subduction earthquakes, empirical models



1. Introduction

Seismic liquefaction is a phenomenon typically generated in loose saturated sandy soils due to an excitation caused by an earthquake. It is “the transformation of granular soil from a solid-state to a liquid state due to increased pore water pressure and reduced effective stress” [1]. Liquefaction produces economic damage and eventual loss of human life [2]. For instance, [3] mention that liquefaction produced severe infrastructure damage during the 1964 Alaska Mw9.2 earthquake. Losses of nearly 80 million dollars and 266 bridges and embankments damaged was reported. Likewise, in the 2010 Maule Mw8.8 earthquake, there were losses of 10538 million dollars in public infrastructure [4], 521 fatalities [5], and 15000 jobs [6].

One of the most dangerous liquefaction-induced ground failures is lateral spreading [7]. These failures generally occur in coastal areas or riverbanks, destroying ports, pavements, and piles bridges. When soil liquefies, non-liquefiable soil layer commonly breaks into large blocks that could move horizontally according along gentle slopes or towards a free face [2].

Many models have been formulated (analytical, empirical, and computational) to study the behavior of liquefiable soil, predict the displacements that can be generated by earthquakes, and evaluate their variation with depth. The purpose has been to provide recommendations for the design of, e.g., foundations and embankments to mitigate losses in the case of future earthquakes [8].

An evaluation of some of empirical models ([9],[10], [11],[12], [2]) was made by [13] and [14] using historical cases of large-magnitude subduction earthquakes. They found weaknesses in those empirical models. Firstly, there was a lack of historical case data with earthquakes of moment magnitudes greater than 8 (the only historical case was the 1964 Alaska Mw9.2 earthquake). Secondly, the term referring to the distance from the site to the seismic source (R) is more challenging when dealing with large magnitude earthquakes. The main aim of this paper is to investigate, using an appropriate numerical model [15], the effects of different geotechnical and seismic parameters in free field conditions on lateral spreading cases for subduction earthquakes.

2. Lateral spreading in short source-to-site distances

In 2014, [13] evaluated six empirical models ([2],[9],[10],[12],[20]) with three cases histories from the 2010 Maule Mw8.8 earthquake and he found that site-to-source distances are difficult to define accurately for large subduction zone earthquakes and that they can vary significantly between seismic regions making it difficult to recommend a method for calculating R. For subduction zones, epicentral distance is impractical because multiple asperities exist for each event, and epicenters are difficult to predict in design.

In the same way, in 2016, [14] used two case histories from the 2010 Maule Mw8.8 earthquake to evaluate empirical methods for predicting lateral spreading for a large magnitude subduction event. She concluded that empirical models ([2], [9]) are extremely sensitive to the distance term R, and the current definition of R for these two methods (Joyner-Boore distance) resulted in predictions that were more than two times the measured values. Furthermore, the empirical model of [20] also predicted displacements roughly 6 to 8 times larger than the measured displacements.

In 2017 [16] studied one case history from the 2010 Maule Mw8.8 earthquake in Caleta Lo Rojas. They used the distance to the zone that bounds 10% of the largest slips in Youd’s equation [2], resulting in satisfactorily values with in-situ post-earthquake measurements.

In this study, we added more sites of lateral spreading from the 2010 Maule Mw8.8 earthquake. The



measured values were between 1 m and 2 m. Figure 1 shows the locations where the lateral spread was measured.

Figure 2 shows a comparison between observed and calculated lateral spreading using Youd's equation [2] with two R-value definitions. The first one is the original R from Youd's equation [2], and the second one is using the distance to the maximum observed coastal uplift. In both cases, we arrived at the same conclusion of [13], [14] and [16] about the problems to use empirical models with large magnitude earthquakes ($M_w > 8$). Finally, the third one shows that R used by [16] neither can predict lateral spread.

3. Verification of the numerical methodology

In this paper, we used Cyclic1D, a finite-element program for one-dimensional dynamic site-response analyses [22]. The software uses a multi-yield-surface plasticity constitutive model [23] to simulate the cyclic mobility response mechanism. We validated the numerical methodology comparing the numerical results against the experimental observation from the centrifuge test of VELACS [24], [25] and LEAP [26] project and field observations from historical cases [16], [18].

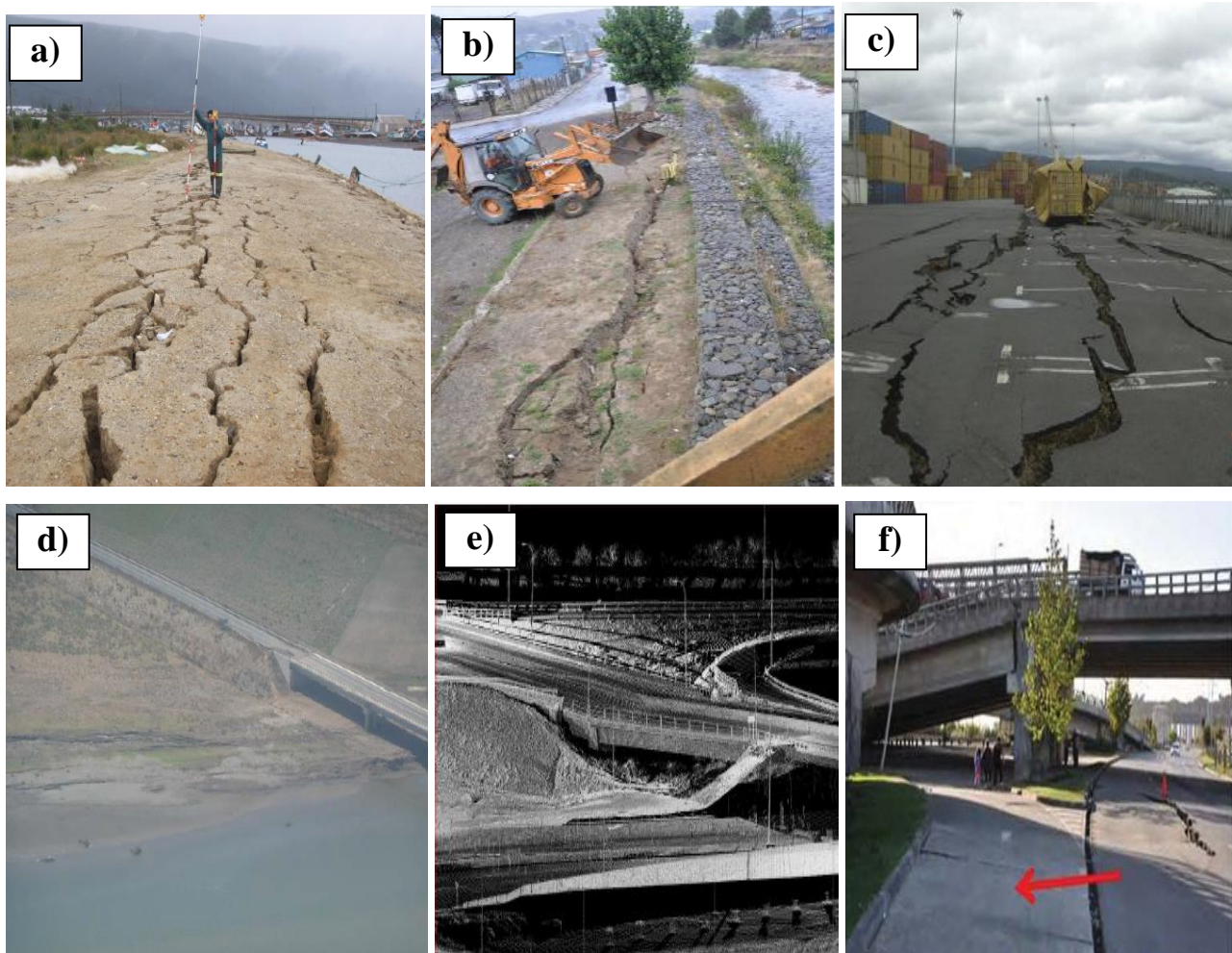


Figure 1. Lateral Spreading observed on a) North river bank Lebu [27] b) Near the river south of the Hospital Provincial in Curanilahue [21] c) Coronel Port [21] d) the north bank of the Mataquito Bridge along the coastal highway [21] e) the north bank of Juan Pablo II bridge [21] f) the north bank of Llacolén bridge [21]

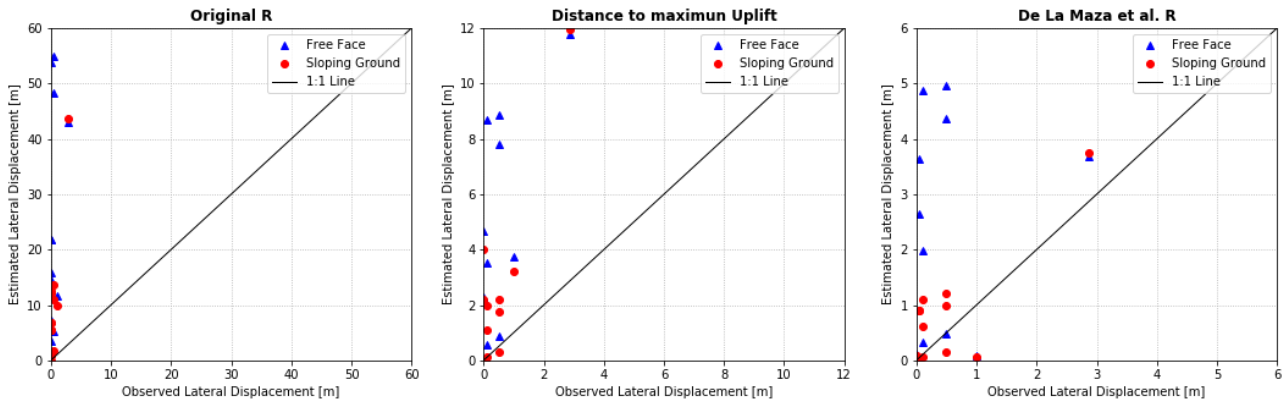


Figure 2. Observed Lateral Displacement versus Estimated Lateral Displacement using a) Original R-value from Youd’s equation [2] b) Distance to Maximum Uplift, and c) Distance under the assumption that the amount of energy released is proportional to the slip magnitude [16]

3.1 Validation with literature centrifuge tests

The numerical methodology [23] has been extensively validated against centrifuge experiments of VELACS and LEAP projects. In this study, we reproduced the same validation model using data form more centrifuge tests [24], [25], and [26].

Figure 3 shows a typical physical model consisting of a 20 cm high, uniform Nevada sand layer with approximately 45% relative density. It is fully saturated with water, inclined 2° with respect to the horizontal. The laminar box is spun at a centrifugal acceleration of 50 g, so the dimensions of the test box and soil permeability coefficient in the prototype scale is 50 times greater than the dimensions and permeability of soil specimen. A target prototype accelerogram is shown in Figure 3 to excite laterally at the base of the physical model.

Likewise, Figure 4 shows a typical physical model consists of a 10 cm high, uniform Ottawa sand layer with approximately 48% relative density. It is fully saturated with water, inclined 5° with respect to the horizontal. The laminar box is spun at a centrifugal acceleration of 30 g, so the dimensions of the test box and soil permeability coefficient in the prototype scale is 30 times greater than the dimensions and permeability of soil specimen. A target prototype accelerogram is shown in Figure 4 to excite laterally at the base of the physical model.

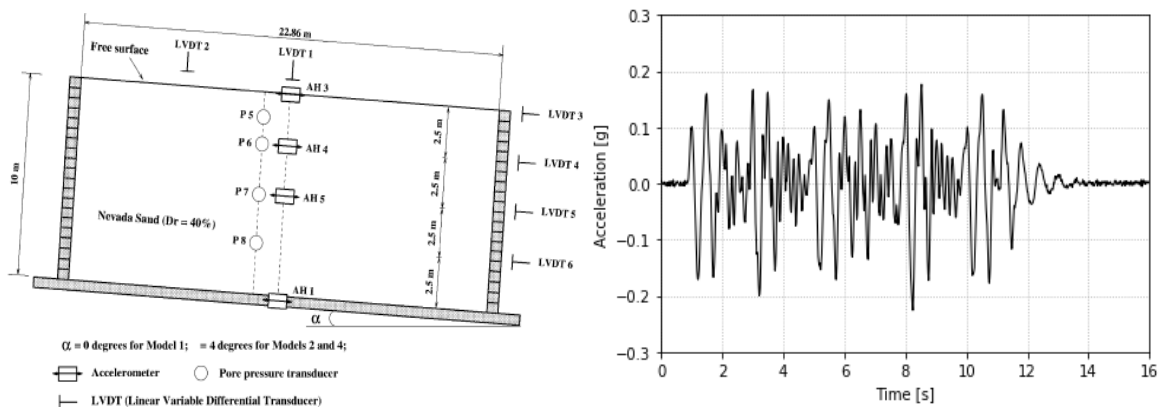


Figure 3. a) General configuration of RPI Centrifuge Model 2 in a laminar container of VELACS project [24] b) lateral Input acceleration at the base of the laminar box [24]

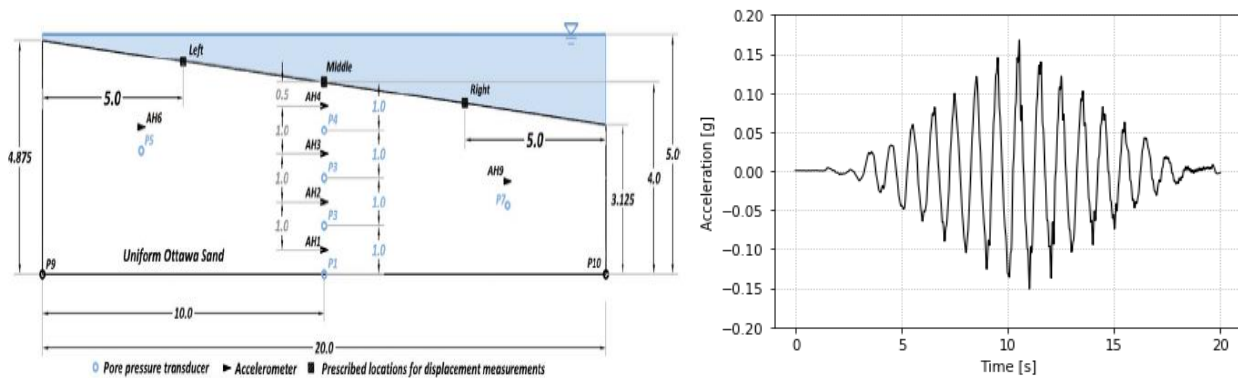


Figure 4. a) General configuration of RPI Centrifuge in the laminar container of LEAP project [24] b) lateral input acceleration at the base of the laminar box [24]

Figure 5 shows a typical comparison between predicted and measured displacements, accelerations, and excess pore pressure time histories from one of the simulated centrifuge tests (M2-2c [24]). The lateral displacements and accelerations obtained from numerical simulation with Cyclic 1D are compatible with the experimental records from RPI Centrifuge Test. In the same way, the excess pore water pressure predicted by the numerical model is also consistent with the experimental records; the maximum value of pore pressure transducers is simulated very well.

Similarly, Figure 6 shows that the results from the numerical simulation with Cyclic 1D is also compatible with the experimental records from the RPI-02 Centrifuge Test from the LEAP project. The excess pore water pressure and acceleration predicted by the numerical model are compatible with the experimental records.

Figure 7 illustrates a summary comparison of the predicted and measured maximum lateral displacement from all centrifuge tests of Table 1. There is a slight overpredicting and underpredicting of the maximum measured displacements. However, in both cases, the numerical model results are reasonably compatible with those from the experimental tests.

Table 1.- Summary of centrifuge test from literature

Test	a_{max} [g]	i [°]	Dr [%]	H [m]	$D_{measured}$ [m]
M1-2 ^a	0.23	0	40-45	10	1.70
M2-2 ^a	0.23	1.94	40-45	10	47.00
M2c-6 ^a	0.17	3.95	40-45	10	72.50
L45V2-10 ^b	0.23	2	45	10	66.00
L65V2-10 ^b	0.20	2	65	10	28.00
L65V2-10 ^b	0.21	2	75	10	23.00
RPI-02 ^c	0.17	5	48	5	35.00

^a [24], ^b [25], [26]^c

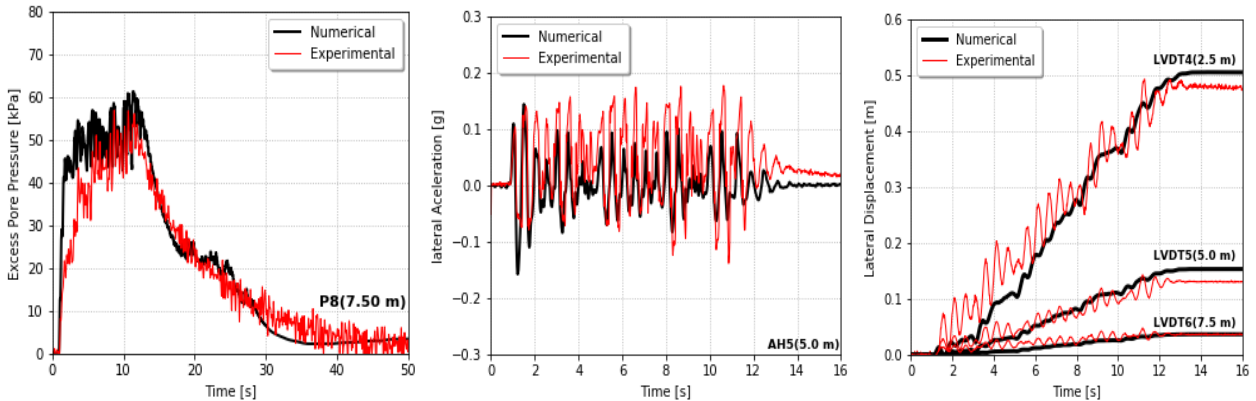


Figure 5. RPI Centrifuge Model 2 recorder and computed with Cyclic 1D a) Excess Pore Pressure time histories, b) Lateral Acceleration time history and c) Lateral Displacement time histories

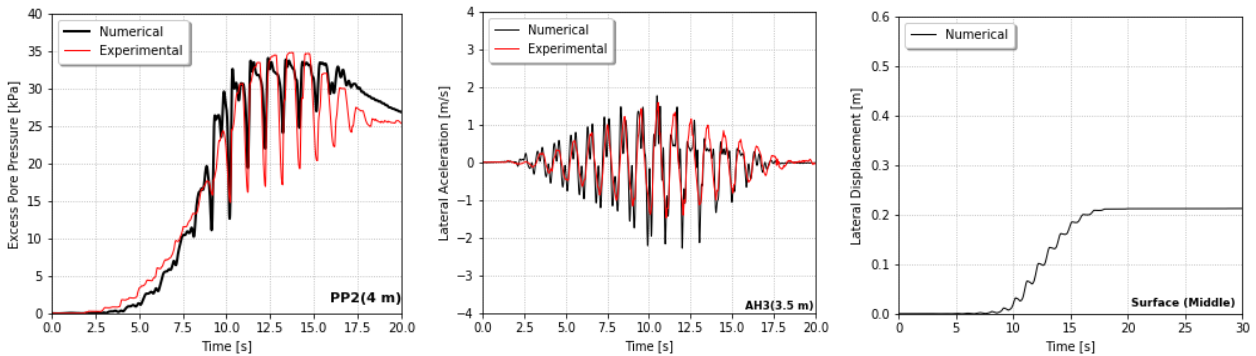


Figure 6. RPI Centrifuge Model 2 recorder and computed with Cyclic 1D a) Excess Pore Pressure time histories, b) Lateral Acceleration time history and c) Lateral Displacement time histories

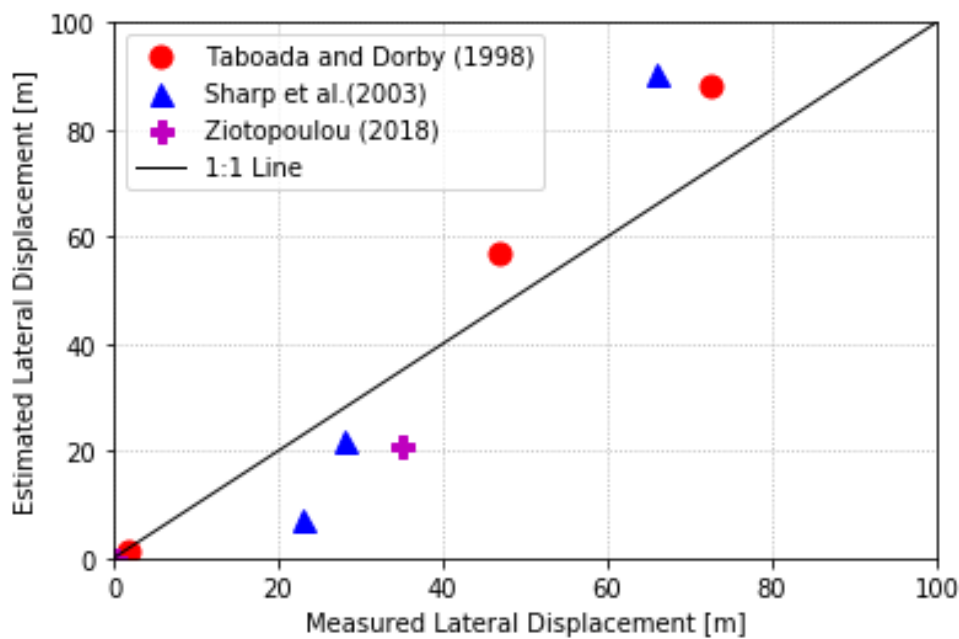


Figure 7. Measured Lateral Displacement from Centrifuge Test versus Estimated Lateral Displacement with Cyclic 1D



3.2 Validation with case histories

In this study, two seismic subduction events with large magnitude are used to reproduce the lateral spreading observed in Lo Rojas Port (2010) and Matanuska River (1964).

3.2.1 The 2010 Maule Mw8.8 earthquake

The 2010 Maule Mw8.8 earthquake caused extensive damage to ports and bridges. Liquefaction-induced lateral spreading significantly damaged the Lo Rojas fishermen port in Coronel, Bío-Bío Region.

Following the criteria of [16], only strong motions recorded in rock stations are adequate for the numerical analyses: RAP (Rapel), COV (Convento), and USM (Santa Maria University). According to the USGS coseismic slip model, the distance to the Lo Rojas site is very similar to the RAP station, which was also close to the site. For that reason, the Rapel (RAP) ground motion was also selected in this study. This station is located around 350 km northeast of Lo Rojas. Figure 8 shows the chosen record with a duration of approximately 90 s and a PGA of 0.2g.

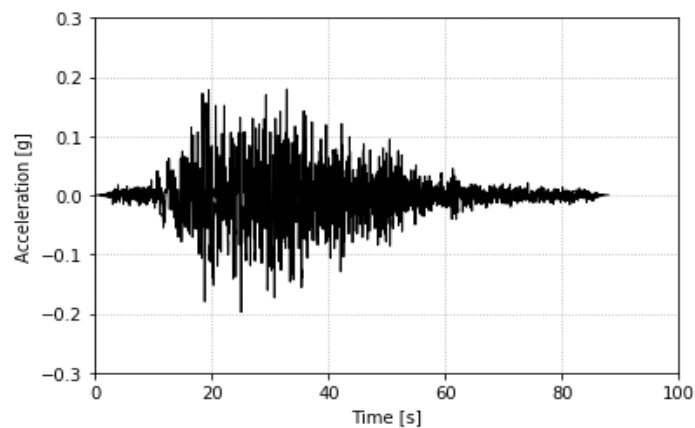


Figure 8. Accelerogram of NS component RA ground motion [16]

3.2.2 The 1964 Alaska Mw9.2 earthquake

The 1964 Alaska Mw9.2 earthquake caused ground failures from lateral spreading [9], collapsing structures, and causing about 130 deaths resulting from the tsunami. According to [17], no strong motion instruments were operated when that destructive seismic event occurred. Therefore, no direct measurement of near-field strong ground motion is available in the form of time histories. Thus, we used a simulated ground motion shared by [17] at the Anchorage site to reproduce the lateral spreading case. Figure 9 shows the selected record with a duration of approximately 250 s and a PGA of 0.25g.

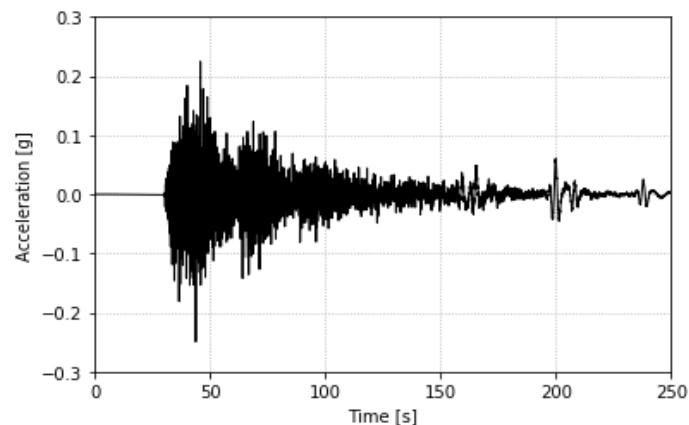


Figure 9. Accelerogram of NS component Anchorage ground motion simulation [17]



To model the lateral spreading, two simplified stratigraphic profiles were selected from the literature ([16],[18]). In both cases, the profiles are in free-field condition. Figure 10 shows the soil stratigraphy of the Lo Rojas and the Matanuska sites.

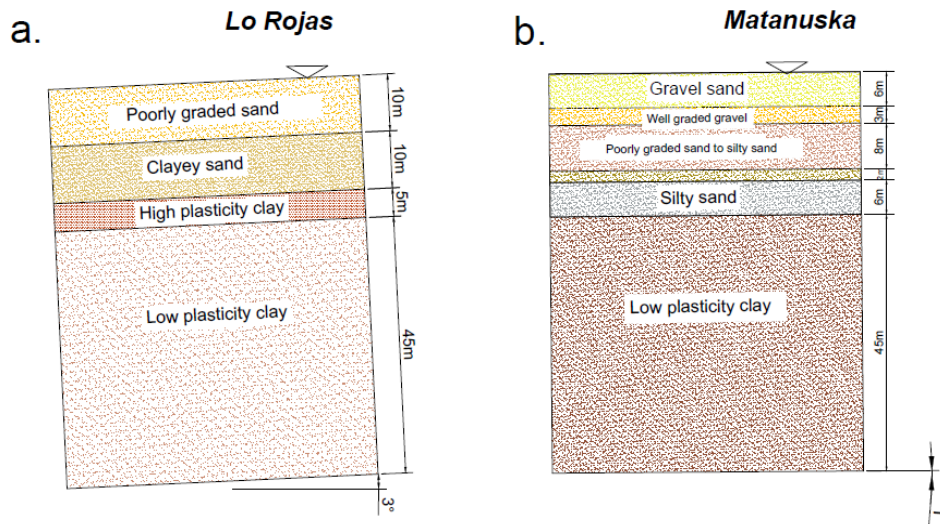


Figure 10. Soil Stratigraphy of liquefaction site in subduction earthquake a. Lo Rojas b. Matanuska

3.2.3 Lo Rojas Site

The same modeling section selected by [16] was used. This geotechnical model was made according to the bathymetry and field test information provided by the Ports Department of the Ministry of Public Works.

According to [18] the geotechnical profile is composed by four soil units: H1 poorly graded sand (about 10 m in thickness), H2 clayey sand (from 11 to 20 m depth), H3 high plasticity clay (5 m thick), H4 low plasticity clay (down to 70 m depth before a highly cemented soil). Table 2 shows the calibrated parameters used for the Lo Rojas model in this study.

Several laboratory tests were conducted to obtain the mechanical parameters for the soil layers: monotonic triaxial, cyclic triaxial, and column shear test (details in [16] and [18]). Using the pore water pressure-based criteria, the numerical results in Figure 11 shows that the H1 soil unit liquefied as the excess pore pressure ratio (r_u) reaches one after 20 seconds during the seismic event.

3.2.3 Matanuska Site

The modeling section was made considering the boreholes taken at the Railroad Bridge Mile Post 147.4 near the Matanuska River [28]. According to [28] the selected geotechnical profile is composed of: gravel sand (about 6 m in thickness), well-graded gravel (from 6 to 8 m depth), poorly graded sand (5 m thick), clayed sand (9 m thick) and low plasticity clay (down to 70 m depth before to find let bottom: a highly cemented soil). Table 3 shows the parameters used in the Matanuska model.

3.2.4 Numerical results

In terms of lateral displacement, the numerical results are reasonably good compared to the field measurements. The observed lateral displacement [16] in Lo Rojas was 2.9 m, which compares well with the numerical result of 2.5 m. Similarly, the maximum observed lateral displacement [2] in Matanuska was 2.5 m which is also similar to the numerical result of 2.8 m.

Figure 11 shows the numerical modeling result of the historical case in terms of acceleration, excess pore pressure ratio, and lateral displacement time history. The excess pore pressure ratio shows the occurrence of liquefaction phenomenon ($r_u=1$).



Table 2.- Mosdel parameters for Lo Rojas site

Unit [USCS]	Depth [m]	γ [kN/m ³]	V_s [m/s]	ρ'_r [kPa]	coeff	k_o	ϕ [°]	γ_r [%]
SP	0-10	19.00	203.3	100	0.5	0.5	31.4	5
CS	11-20	19.99	223.7	80	0.5	0.67	35	5
CH	21-25	19.99	223.7	80	0.5	0.67	35	5
CL	25-70	21.00	253.5	80	0.5	0.67	40	5
Unit [USCS]	PT [°]	c_1	c_2	d_1	d_2	liq	K [m/s]	NYS
SP	26.5	0.19	0.19	0.2	10	0.015	3.3E-5	25
CS	26.5	0.12	0.2	0.2	10	0.015	6.6E-5	20
CH	24	0.06	0.5	0.4	10	0.01	1E-7	20
CL	22	0.01	0.6	0.6	10	0.003	6.6E-05	40

Table 3. - Model parameters for Matanuska site

Unit [USCS]	Depth [m]	γ [kN/m ³]	V_s [m/s]	ρ'_r [kPa]	coeff	k_o	ϕ [°]	γ_r [%]
SG	0-6	1900	203.3	100	0.5	0.5	31.6	5
GW	6-8	1900	203.3	80	0.5	0.67	31.4	5
SP	9-16	1900	203.3	80	0.5	0.67	31.4	5
SC	17-26	1999	223.7	80	0.5	0.67	31.4	5
CL	27-70	1300	100	80	0.5	0.67	40	5
Unit [USCS]	PT [°]	c_1	c_2	d_1	d_2	liq	K [m/s]	NYS
SG	0-6	0.19	0.2	0.2	10	0.015	1.2E-3	
GW	6-8	0.19	0.2	0.2	10	0.015	1.0E-7	20
SP	9-16	0.19	0.2	0.2	10	0.015	6.6E-5	20
SC	17-26	0.06	0.5	0.4	10	0.01	6.6E-5	20
CL	27-70	-	-	-	-	-	1.0E-9	20

4. Lateral spreading versus different Ground Motion Intensity Parameters

Once the numerical model was validated, a 10 m liquefiable soil layer was modeled with an inclination of 2°. Different input ground motions from large-magnitude subduction earthquakes were used and scaled to 0.113g, 0.226g, and 0.339g. The scaled input records were from the 2010 Maule, 2104 Iquique, and VELACS project. The numerical modeling was made in Cyclic1D with the same conditions as the centrifugal test modeling. The purpose was to obtain the maximum lateral displacement on the surface and correlate it with different ground motion intensity measures. Figure 13 shows that the most influential parameters are,



for the analyzed cases, Cumulative Absolute Velocity (CAV), Peak Ground Velocity (PGV) and Arias Intensity (AI).

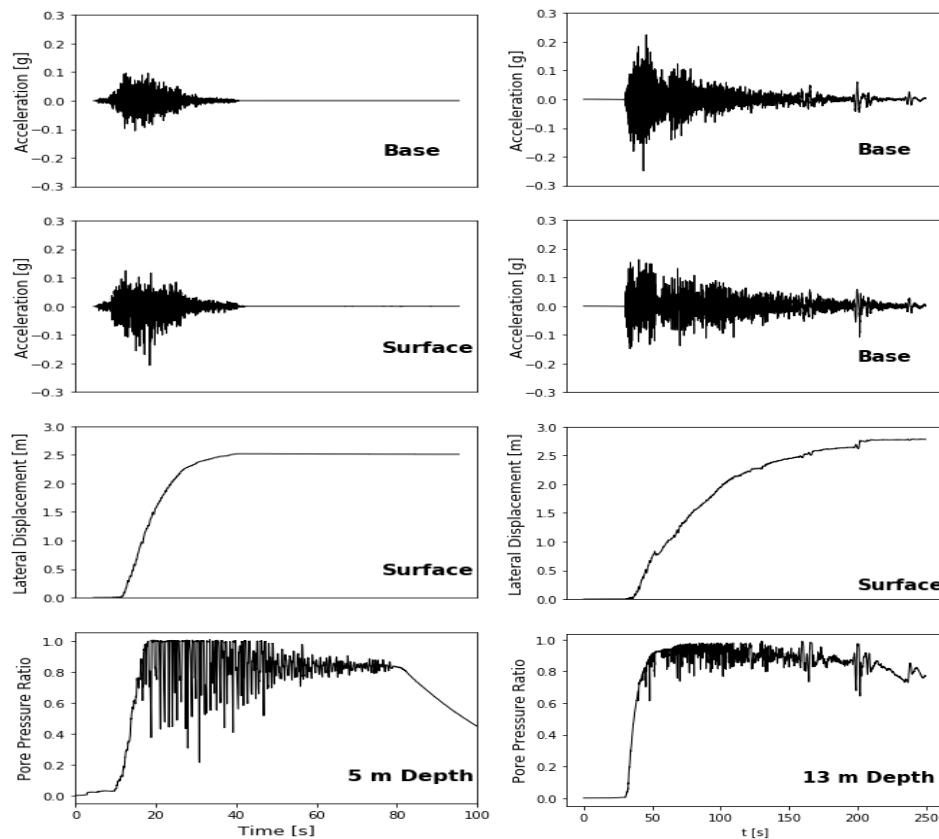


Figure 11. Numerical modeling results

The following acronyms are used in Figure 12: AI= Arias Intensity, Ic=Intensity Characteristic, SED= Specific Energy Density, CAV= Cumulative Absolute Velocity, ASI= Acceleration Spectrum Intensity, VSI= Velocity Spectrum Intensity, HI= Housner Intensity, SMA= Sustained Maximum Acceleration, SMV=Sustained Maximum Velocity, EDA= Effective Design Acceleration, A95 =Threshold of Acceleration when 95% of AI is achieved, Tp=Predominant Period, Tm=Mean Period, SD=Significant Duration, UD=Uniform Duration, BD=Bracketed duration, PGV= Peak Ground Velocity, PGD=Peak Ground Displacement, Vmax/Amx=Ratio of Maximum Velocity and Maximum Acceleration, Arms= Root-Mean-Square Acceleration

5. Conclusions

Based on the results of the parametric study, the findings can be summarized as follows:

- Defining a source-to-site distance for large-magnitude subduction earthquakes to be used in empirical formulas is still problematic.
- Cyclic1D is a numerical tool that reproduces consistent results to evaluate liquefaction-induced by lateral displacement in subduction cases.
- CAV, PGV, and AI show a good correlation with lateral spreading from the analyzed subduction earthquake cases.

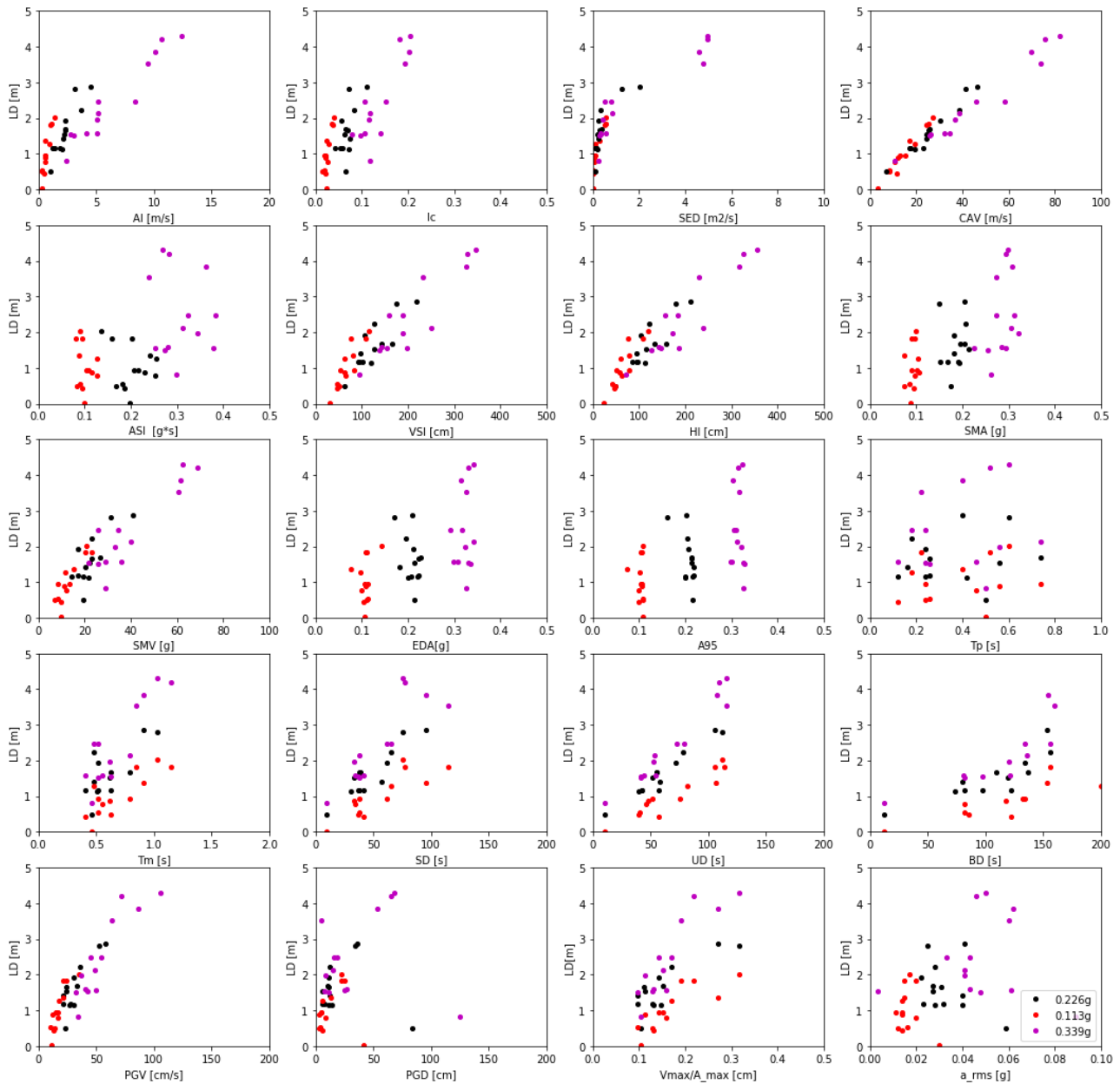


Figure 12. Relationship between the selected GMI's and Lateral Displacement

6. Acknowledgments

The authors wish to thank Prof. Ahmed Elgamal for providing his feedback during the numerical analyses and thank the Chilean Ministry of Public Works for allowing the use of its photographic material.

7. References

- [1] Committee on Soil Dynamics. (1978). Definition of terms related to liquefaction. *Journal of Geotechnical Engineering Div.*, 104, 1197–2000.
- [2] Youd, L., Hansen, C., Bartlett, S. (2002). Revised Multilinear Regression Equations for Prediction of Lateral Spread Displacement. *Journal of Geotechnical and Geoenvironmental Engineering*, 128 (December), 1007–1017.
- [3] Franke, K., Rollins, K. (2017). Lateral Spread Displacement and Bridge Foundation Case Histories from the 1991 Magnitude. *Journal of Geotechnical and Geoenvironmental Engineering*, 143(6), 1–16.



- [4] Contreras, M. y Winckler, P. (2013). Pérdidas de vidas, viviendas, infraestructura y embarcaciones por el tsunami del 27 de Febrero de 2010 en la costa central de Chile. *Obras y Proyectos* 14, 6-19.
- [5] Fritz, H., Petroff, C., Catalán, P., Cienfuegos, R., Winckler, P., Kalligeris, N., Weiss, R., Barrientos, S., Meneses, G., Valderas-Bermejo, C., Ebeling, C., Papadopoulos, A., Contreras, M., Almar, R., Dominguez, J. and Synolakis, C. (2011). Field Survey of the 27 February 2010 Chile Tsunami. *Pure and Applied Geophysics* 168: 1989–2010
- [6] EERI (2010). Mw 8.8. Chile Earthquake of February 27, 2010. Special Earthquake Report. http://www.eeri.org/site/images/eeri_newsletter/2010_pdf/Chile10_insert.pdf. April 2013
- [7] Youd, L. (2018). Application of MLR Procedure for Prediction of Liquefaction-Induced Lateral Spread Displacement. *Journal of Geotechnical and Geoenvironmental Engineering*, 144(6), 04018033.
- [8] Valsamis, A., Bouckovalas, G., Papadimitriou, A. (2010). Parametric investigation of lateral spreading of gently sloping liquefied ground. *Soil Dynamics and Earthquake Engineering*, 30(6), 490–508.
- [9] Bartlett, S., Youd, L. (1995). Empirical Prediction of Liquefaction-Induced Lateral Spread. *Journal of Geotechnical Engineering*, Vol. 121, No. 4.
- [10] Faris, A., Seed, B., Kayen, R., Wu, J. (2006). A Semi-Empirical Model for the Estimation of Maximum Horizontal Displacement Due to Liquefaction-Induced Lateral Spreading. *Proceedings of the 8th U.S. National Conference on Earthquake Engineering*, paper 1323, San Francisco.
- [11] Rauch, A. F., and Martin, J. R., 2000. EPOLLS Model for Predicting Average Displacement Lateral Spreads, *Journal of Geotechnical and Geoenvironmental Engineering*, Vol. 126, No. 4.
- [12] Zhang, J., Changwei, Y., Zhao, J., McVerry, G., (2012). Empirical Models for Predicting Lateral Spread Considering the Effects of Regional Seismicity, *Earthquake Engineering, and Engineering Vibrations*, vol. 11, No. 1, pp. 121-131.
- [13] Tryon, G. (2014). Evaluation of Current Empirical Methods for Predicting Lateral Spread-Induced Ground Deformations for Large Magnitude Earthquakes Using Maule Chile 2010 Case s. *All Theses and Dissertations*. 5852.
- [14] Williams, N. (2015). Evaluation of Empirical Prediction Methods for Liquefaction-Induced Lateral Spread from the 2010 Maule, Chile, Mw 8.8 Earthquake in Port Coronel. *All Theses and Dissertations*. 6086
- [15] Elgamal, A., Yang, Z., & Parra, E. (2002). Computational modeling of cyclic mobility and post-liquefaction site response. *Soil Dynamics and Earthquake Engineering*, 22, 259–271.
- [16] De la Maza, G., Williams, N., Sáez, E., Ledezma, C. (2017). Liquefaction-Induced Lateral Spread in Lo Rojas, Coronel, Chile: Field Study and Numerical Modeling. *Earthquake Spectra*, 33(1), 219–240.
- [17] Mavroeidis, G. P., B. Zhang, G. Dong, A. S. Papageorgiou, U. Dutta, and N. N. Biswas (2008). Estimation of strong ground motion from the Great 1964 Mw 9.2 Prince William Sound, Alaska, earthquake, *Bulletin of the Seismological Society of America*, Vol. 98, No. 5, pp. 2303-2324.
- [18] Gillins, D., Bartlett, S. (2014). Multilinear regression equations for predicting lateral spread displacement from soil type and cone penetration test data. *Journal of Geotechnical and Geoenvironmental Engineering*, 140(4), 1–11.
- [19] Barrueto, C., Sáez, E., Ledezma, C. (2017). Seismic demand on piles in sites prone to liquefaction-induced lateral spreading. *Seismic Performance of Soil-Foundation-Structure Systems - Selected Papers from the International Workshop on Seismic Performance of Soil-Foundation-Structure Systems*, 2016, 171–182.
- [20] Zhang, G., Robertson, P., Brachman, R. (2004). Estimating Liquefaction-Induced Lateral Displacements Using the Standard Penetration Test or Cone Penetration Test, *Journal of Geotechnical and Geoenvironmental Engineering*, Vol. 130, No. 8, pp. 861-871.
- [21] GEER. (2010). Geo-engineering Reconnaissance of the 2010 Maule, Chile Earthquake.
- [22] Yang Z., Lu J., Elgamal A. (2004). A Web-Based a Platform for computer simulation of seismic ground response. *Advanced Engineering Software*; 35(5):249–59.
- [23] Elgamal, A., Yang, Z., Parra, E. (2002). Computational modeling of cyclic mobility and post-liquefaction site response. *Soil Dynamics and Earthquake Engineering*, 22, 259–271.
- [24] Taboada V., Dobry R. (1998). Centrifuge modeling of earthquake-induced lateral spreading in sand. *Journal of Geotechnical and Geoenvironmental Engineering*. ASCE; 124(12):1195–206.
- [25] Sharp M., Dobry R. (2002) Sliding block analysis of lateral spreading based on centrifuge results. *International Journal of Physical Model Geoenvironmental*; 2:13–32.
- [26] Ziopoulou, K. (2018). Seismic response of liquefiable sloping ground: Class A and C numerical predictions of centrifuge model responses. *Soil Dynamics and Earthquake Engineering*, 113(December 2015), 744–757.
- [27] Ministerio de Obras Públicas. Photograph taken by Luis Lopez Carrasco. Gobierno de Chile (2010).
- [28] Bartlett, S., Youd, L. (1992). Empirical Analysis of Horizontal Ground Displacement Generated by Liquefaction-Induced Lateral Spreads by. National Center for Earthquake Engineering Research. Wu, J., Kammerer, A. M., Riemer, M. F., Seed, R. B., and Pestana, J. M. (2004). 13th World Conference on Earthquake Engineering (p. 14).ssss